



Optimal vehicle position estimation using adaptive unscented Kalman filter based on sensor fusion*

Giseo Park^{*}

School of Mechanical Engineering, University of Ulsan, Ulsan 44610 Korea



ARTICLE INFO

Edited by Dr. Yan Chen

Keywords:

Adaptive unscented kalman filter
Sensor fusion
Vehicle position
Global positioning system
inertial measurement unit

ABSTRACT

Precise position recognition systems are actively used in various automotive technology fields such as autonomous vehicles, intelligent transportation systems, and vehicle driving safety systems. In line with this demand, this paper proposes a new vehicle position estimation algorithm based on sensor fusion between low-cost standalone global positioning system (GPS) and inertial measurement unit (IMU) sensors. In order to estimate accurate vehicle position information using two complementary sensor types, adaptive unscented Kalman filter (AUKF), an optimal state estimation algorithm, is applied to the vehicle kinematic model. Since this AUKF includes an adaptive covariance matrix whose value changes under GPS outage conditions, it has high estimation robustness even if the accuracy of the GPS measurement signal is low. Through comparison of estimation errors with both extended Kalman filter (EKF) and UKF, which are widely used state estimation algorithms, it can be confirmed how improved the estimation performance of the proposed AUKF algorithm in real-vehicle experiments is. The given test course includes roads of various shapes as well as GPS outage sections, so it is suitable for evaluating vehicle position estimation performance.

1. Introduction

Global positioning system (GPS) is the most widely used navigation device that can recognize its own position outdoors in real time [1]. However, standard commercial GPS causes major problems in terms of sensor accuracy in GPS outage areas where satellite reception is difficult, such as around tall buildings or in tunnels [2]. In addition, the lower the price of the standalone GPS, the lower the measurement sampling rate. There is a trade-off relationship between price competitiveness and measurement accuracy about the standalone GPS [3]. Therefore, in high-speed cornering situations, this low sampling rate leads to inaccurate vehicle position information, which has the potential to cause confusion to the driver.

Accordingly, sensor fusion between the standalone GPS and other sensors is being developed as a solution to a highly reliable vehicle position recognition system [4,5]. In particular, the inertial measurement unit (IMU) sensor has the following characteristics and has high complementarity with the standalone GPS [6–8]. 1) Compared to low-cost standalone GPS, it has a much higher measurement sampling rate (up to 100 Hz). 2) IMU sensors are not affected by the surrounding

environment, except for temperature. 3) When the acceleration and angular velocity signals measured from the IMU sensor are directly integrated, the velocity and angle including the integrated drift due to offset are output.

Accordingly, vehicle position estimation using sensor fusion between standalone GPS and IMU sensors is also actively utilized in automotive application fields (autonomous driving systems, advanced driver assistance systems (ADAS), intelligent transportation systems (ITS), chassis safety control systems, etc.) [9].

1.1. Literature review

Previous studies on vehicle position estimation using sensor fusion of standalone GPS and IMU sensors are as follows. Fuzzy logic technique for GPS dead reckoning was proposed in [10] and a low-cost vehicle localization system well-behaved even at very low vehicle speed was designed by Bonnabel et al. [11], respectively. Also, the vehicle positioning system in [2] actively utilized the vehicle lateral dynamic model to complement the vehicle kinematic model. In addition, various existing methods are summarized along with each main algorithm and

* This paper was recommended for publication by Associate Editor Dr. Yan Chen

* Corresponding author.

E-mail address: eloq123@ulsan.ac.kr.

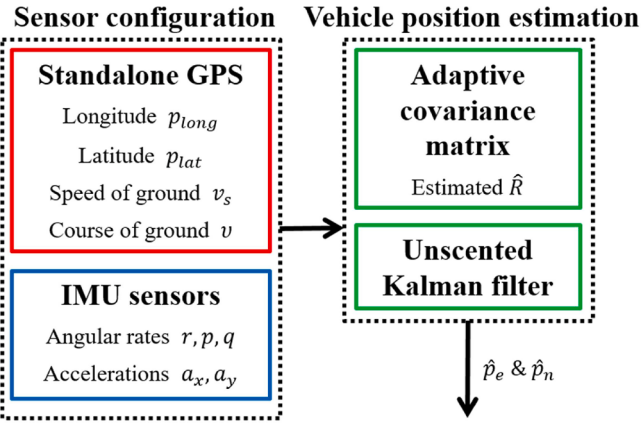
Table 1

Various existing vehicle positioning methods using GPS and IMU sensors.

Ref.	Main estimation algorithm	Features
[12]	Extended Kalman filter (EKF)	Tightly coupled scheme using GPS and IMU sensors - Pros : Abnormal GPS measurement elimination to achieve continuous vehicle position - Cons : Error occurrence during model linearization process
[13]	Autoregressive and moving average (ARMA)	Prediction models based on ARMA - Pros : Using occupancy grid constraints for improved accuracy - Cons : Requires a lot of computational burden
[14]	Non-Gaussian delayed particle smoother	Including ensemble Kalman filter as a computation approach - Pros : Considering non-Gaussianity of the measurement and process noises - Cons : Reduction in computation time is required
[15]	Machine learning	Combining EKF with machine learning techniques - Pros : Improving the accuracy during GPS failure - Cons : Field driving data set needs to be updated
[16]	Interacting multiple model (IMM) approach	Updating in the prediction stage of IMM - Pros : Credibilistic way with the likelihood model - Cons : Probability transition parameters are set only based on experience
[3,17]		Using GPS and in-vehicle sensors - Pros : Combination between vehicle dynamic and kinematics models - Cons : In-vehicle sensors have relatively low measurement accuracy
[18]		Using IMM-based UKF - Pros : Including Grey neural network module for improvement of estimation accuracy - Cons : Uncertainty in vehicle model parameters
[19]	Particle filter	Based on particle swarm optimization - Pros : Combining the sensor data and digital maps - Cons : Sophisticated digital map information is essential
[20]		Hybridization of the particle filter by particle swarm optimization - Pros : Robust to noises such as GPS multipath - Cons : Computational burden increases depending on the number of particles
[21–23]	unscented Kalman filter (UKF)	Utilizing a deterministic sampling technique known as an unscented transformation - Pros : High estimation accuracy in nonlinear models - Cons : Noise covariance matrix is determined only by experience

features in Table 1.

The points that can be checked from these existing studies are as follows. First, when using a lateral dynamic model as a vehicle model, it is difficult to respond to the uncertainty of various vehicle parameter information such as total vehicle mass, yaw moment of inertia and tire stiffness values. Accordingly, a kinematic model that does not include any vehicle parameters is robust to inaccuracy in these vehicle parameters. The second point is the nonlinearity that occurs when expressing GPS measurement values (vehicle speed and course angle) on a vehicle fixed coordinate system. This makes it hard to apply linear system estimators such as Luenberger observer and linear Kalman filter to GPS measurements.

**Fig. 1.** Overall algorithm architecture.

1.2. Overview

This paper deals with the estimation of vehicle position using the sensor fusion of IMU sensors and standalone GPS. As mentioned above, a common limitation of previous studies is the decrease in accuracy of vehicle position estimation due to the nonlinearity on vehicle body coordinates of GPS measurement information. To solve this problem, a vehicle position estimation algorithm using the adaptive unscented Kalman filter (AUKF) is newly proposed in this paper, as shown in Fig. 1.

Compared to existing AUKF-based position estimation methods [24–26], the AUKF proposed in this paper has the following characteristics. It is based on the general UKF and is accompanied by adaptive covariance matrix of measurement noise \hat{R} that changes to appropriate values depending on the situation. In particular, by quickly increasing the magnitude of each element within the matrix \hat{R} in the GPS outage section where GPS measurement accuracy drops sharply, the proposed AUKF can quickly reduce the weight of GPS measurements. At this time, this adaptive covariance matrix is calculated in real time through linearization of the nonlinear model. As a result, the proposed AUKF can output the accurately estimated vehicle position while considering the nonlinearity of the vehicle system and GPS measurement models.

1.3. Contributions

The contributions where the vehicle position estimation algorithm proposed in this paper can be differentiated from the existing ones are summarized as follows.

- 1) The value of noise covariance matrix related to the measurement error is quickly adjusted while detecting the GPS outage condition in which the accuracy of the GPS measurement signal rapidly decreases. Accordingly, the AUKF has high robustness of vehicle position estimation even in GPS outage conditions.
- 2) As the average filter is newly applied in the process of calculating the adaptive covariance matrix of the AUKF, it is possible to control how quickly this adaptive covariance matrix can change.
- 3) In order to improve the accuracy of the vehicle kinematics model, the 3-D motion of the vehicle, i.e. roll and pitch motions, are considered together in the AUKF.

This paper is composed of six sections. The sensor configuration is explained in Section II. Also, Section III describes the vehicle kinematic model. Then, Section IV focuses on the AUKF for the vehicle position estimation. In Section V, the proposed estimation algorithm is validated through experiments. Finally, Section VI concludes the paper.

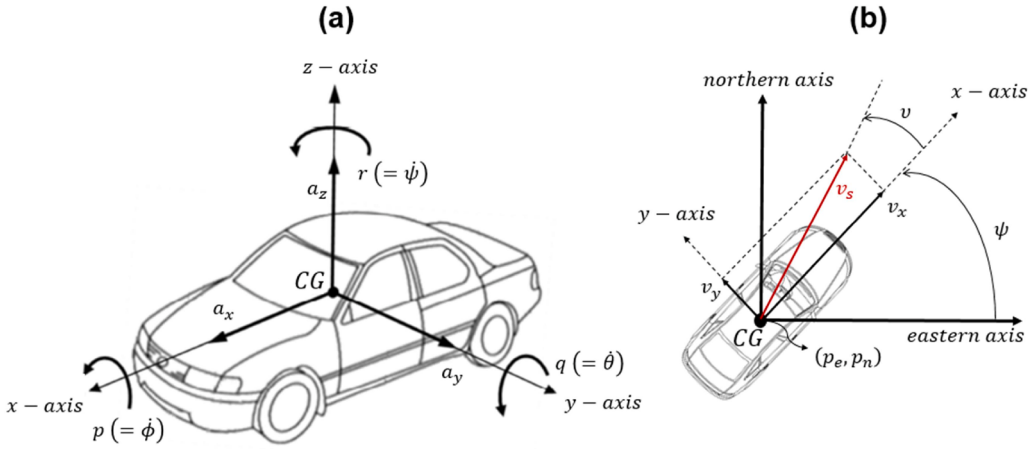


Fig. 2. Vehicle kinematic model: (a) Body-fixed coordinate system and (b) Earth-fixed coordinate system.

2. Sensor configuration

Since the development of a practical vehicle position estimation algorithm with high price competitiveness is the main purpose, a low-cost standalone GPS with a sampling frequency of 1 Hz and IMU sensors with a relatively fast sampling frequency of 100 Hz are used simultaneously for sensor fusion.

2.1. IMU sensors

In this paper, the dual-axis accelerometer (ADXL203 from Analog Devices, Inc.) measure longitudinal a_x and lateral accelerations a_y at the vehicle center of gravity (CG), respectively. Also, angular rates r , p , and q for the three axes are output through respective gyroscopes (ADW22307 from Analog Devices, Inc.). At this time, the angular rates about the x , y , and z axes match the vehicle roll rate, pitch rate, and yaw rate, respectively. Thanks to these IMU sensors (one accelerometer and three gyroscopes), accuracy of vehicle position estimation in Section IV can be maintained even in high-speed cornering situations with severe lateral slip [27].

2.2. Standalone GPS

In order to develop a vehicle position estimation system with price competitiveness [5], MiniGmouse from AscenKorea, Inc., which is in a relatively low price range, is utilized as the standalone GPS receiver in this paper. The outputs of the GPS are as follows.

- Latitude p_{lat} and longitude p_{long} in the world geodetic system: these can be converted into earth-fixed coordinate system with northern and eastern axes as follows.

$$p_{n_GPS} = k_{lat}(p_{lat} - p_{o,lat}) \quad (1)$$

$$p_{e_GPS} = k_{long}(p_{long} - p_{o,long}) \quad (2)$$

where $p_{o,lat}$ and $p_{o,long}$ are the latitude and longitude at the origin position; k_{lat} and k_{long} the constant proportional factors (However, for very large driving areas, they are expressed as a function of latitude and longitude [28]); and p_{n_GPS} and p_{e_GPS} the vehicle positions on northern and eastern axes measured by the GPS, respectively.

- Vehicle speed on plane v_s : it is also called the speed of ground.
- Course angle on plane v : this denotes the direction of the velocity vector on northern and eastern axes.

Based on the GPS Doppler shift and the line-of-sight between the vehicle and the satellite, these vehicle speed and course angle are calculated [29].

- Number of satellites (NS) and horizontal dilution of precision (HDOP): These are closely related to the measurement accuracy of GPS, and by observing their changes, GPS outages can be detected [30].

3. Vehicle kinematic model

Figs. 2(a) and (b) present the vehicle kinematic model in body-fixed and earth-fixed coordinate systems, respectively. In particular, Fig. 2(b) shows the northern and eastern axes for GPS and the longitudinal (x) and lateral (y) axes for IMU sensors at the same time. The equations of the vehicle kinematic model in a two-dimensional plane are expressed as follows [7]:

$$\dot{p}_n = v_x \sin(\psi) + v_y \cos(\psi) \quad (3)$$

$$\dot{p}_e = v_x \cos(\psi) - v_y \sin(\psi) \quad (4)$$

$$\dot{v}_x = rv_y + a_{x_com} \quad (5)$$

$$\dot{v}_y = -rv_x + a_{y_com} \quad (6)$$

$$\dot{\psi} = r \quad (7)$$

where ψ , v_x and v_y are yaw angle, vehicle longitudinal and lateral velocities, respectively. Also, the compensated vehicle accelerations considering the vehicle attitude (roll ϕ and pitch angles θ) are $a_{x_com} = a_x + g\sin(\theta)$ and $a_{y_com} = a_y - g\sin(\phi)\cos(\theta)$.

Furthermore, v_n and v_e , which represent the vehicle velocities on the northern and eastern axes, can be expressed as follows through GPS measurements (v_s and v):

$$v_n = v_s \sin(v) = v_x \sin(\psi) + v_y \cos(\psi) \quad (8)$$

$$v_e = v_s \cos(v) = v_x \cos(\psi) - v_y \sin(\psi) \quad (9)$$

By integrating (3) to (7), the state space equation can be defined as continuous systems: $\dot{x} = f(x, u)$ and $y = h(x)$ where the state vector $x = [p_n \ p_e \ v_x \ v_y \ \psi]^T$, the input vector $u = [a_{x_com} \ a_{y_com} \ r]^T$, the measurement vector $y = [p_{n_GPS} \ p_{e_GPS} \ v_n \ v_e]^T$,

$$f(x, u) = \begin{bmatrix} v_x \sin(\psi) + v_y \cos(\psi) \\ v_x \cos(\psi) - v_y \sin(\psi) \\ rv_y + a_{x_com} \\ -rv_x + a_{y_com} \\ r \end{bmatrix} \text{ and } h(x) = \begin{bmatrix} p_n \\ p_e \\ v_x \sin(\psi) + v_y \cos(\psi) \\ v_x \cos(\psi) - v_y \sin(\psi) \end{bmatrix}.$$

To determine the observability of given n -state nonlinear systems $\dot{x} = f(x, u)$ and $y = h(x)$, the Lie derivative function $L_f^{(i)}$ and the observability function O are utilized.

$$O = \begin{bmatrix} \frac{\partial L_f^{(0)}}{\partial x} \\ \frac{\partial L_f^{(1)}}{\partial x} \\ \vdots \\ \frac{\partial L_f^{(n-1)}}{\partial x} \end{bmatrix} \quad (10)$$

$$L_f^{(i)} = \begin{cases} h & (i=0) \\ \frac{\partial L_f^{(n-1)}}{\partial x} f & (i=1, \dots, n-1) \end{cases} \quad (11)$$

As stated in Appendix, the observability function O in (10) has a full rank of n (number of state variables) in this paper, it is verified that these nonlinear systems are locally observable except when the vehicle is at rest: $v_x = 0$.

4. Vehicle position estimation

The Kalman filter is known to be able to derive optimal state variable estimation based on probability statistics, and is one of the methodologies widely used in vehicle state estimation research. Especially, the AUKF uses an unscented transformation to select the minimal set of sigma points around the mean.

Sigma points are propagated through a nonlinear function, which allows new mean and covariance estimates to be formed. Therefore, the results vary depending on the transformed statistical calculation of the unscented transformation and the sigma point set used. It should be noted that it is always possible to construct a new AUKF in a consistent way. The resulting AUKF provides more accurate estimates of true means and covariances.

4.1. AUKF design

The vehicle kinematic model equations introduced in Section III above are applied to AUKF. First, the nonlinear systems can be expressed as the following discrete model equations:

$$x_{k+1} = f_d(x_{k-1}, x_k, u_k) + w_k \quad (12)$$

$$y_k = h(x_k) + v_k \quad (13)$$

where $f_d(x_k, u_k) = x_{k-1} + T_s f(x_k, u_k)$ and T_s is the given sampling time. Also, the system process noise w_k and the measurement noise v_k (uncorrelated white sequences including zero means) have the covariance matrices Q_k and R_k , respectively: i.e., $w_k \sim (0, Q_k)$ and $v_k \sim (0, R_k)$.

Next, the following time update equations are utilized to derive the priori estimate \hat{x}_k^- and the priori error covariance P_k^- . Then, choose sigma points:

$$\hat{x}_{k-1}^{(i)} = \hat{x}_{k-1}^+ + \sqrt{(n+\lambda)P_{k-1}^+} \quad (i=1, \dots, n) \quad (14)$$

$$\hat{x}_{k-1}^{(i)} = \hat{x}_{k-1}^+ - \sqrt{(n+\lambda)P_{k-1}^+} \quad (i=n+1, \dots, 2n) \quad (15)$$

where $\lambda = \alpha^2(n+k_i) - n$ (here, α and k_i are scale parameters). Then, derive \hat{x}_k^- at time k with $\hat{x}_k^{(i)} = f(\hat{x}_{k-1}^{(i)}, u_k)$.

$$\hat{x}_k^- = \frac{1}{2n} \sum_{i=1}^{2n} \omega_m^{(i)} \hat{x}_k^{(i)} \quad (16)$$

At this time, $\omega_m^{(i)}$ and $\omega_c^{(i)}$ are the mean weight and variance weight of the i -th sigma point, respectively. They can be defined as follows:

$$\omega_m^{(i)} = \begin{cases} \frac{\lambda}{n+\lambda} & (i=0) \\ \frac{0.5}{n+\lambda} & (i=1, \dots, 2n) \end{cases} \quad (17)$$

$$\omega_c^{(i)} = \begin{cases} \frac{\lambda}{n+\lambda} & (i=0) \\ \frac{0.5}{n+\lambda} + 1 - \alpha^2 + \beta & (i=1, \dots, 2n) \end{cases} \quad (18)$$

Here, β is the scale parameter. Also, P_k^- can be derived as follows.

$$P_k^- = \sum_{i=1}^{2n} \omega_c^{(i)} (\hat{x}_k^{(i)} - \hat{x}_k^-) (\hat{x}_k^{(i)} - \hat{x}_k^-)^T + Q_{k-1} \quad (19)$$

These (14) to (19) correspond to the time update step, and the measurement update step proceeds next. The predicted measurement at time k with $\hat{y}_k^{(i)} = h(\hat{x}_k^{(i)})$ can be given as

$$\hat{y}_k = \sum_{i=1}^{2n} \omega_m^{(i)} \hat{y}_k^{(i)}. \quad (20)$$

Then, the covariance of the predicted measurement $\hat{y}_k^{(i)}$ is expressed as follows.

$$P_y = \sum_{i=1}^{2n} \omega_c^{(i)} (\hat{y}_k^{(i)} - \hat{y}_k) (\hat{y}_k^{(i)} - \hat{y}_k)^T + R_k \quad (21)$$

Also, the cross covariance between \hat{x}_k^- and \hat{y}_k is given as

$$P_{xy} = \sum_{i=1}^{2n} \omega_c^{(i)} (\hat{x}_k^{(i)} - \hat{x}_k^-) (\hat{y}_k^{(i)} - \hat{y}_k)^T. \quad (22)$$

Finally, the Kalman gain K_k , the posteriori estimate \hat{x}_k^+ and the posteriori error covariance P_k^+ are derived as following equations.

$$K_k = P_{xy} P_y^{-1} \quad (23)$$

$$\hat{x}_k^+ = \hat{x}_k^- + K_k (y_k - \hat{y}_k) \quad (24)$$

$$P_k^+ = P_k^- - K_k P_y K_k^T \quad (25)$$

4.2. Adaptive covariance matrix

The estimation accuracy of the Kalman filter depends on system model reliability and measurement precision. The noise covariance matrices of existing Kalman filters are generally set to constant values for convenience [10]. This lack of flexibility in the noise covariance matrix can lead to poor performance in worst-case scenarios. [31]. To overcome these limitations of the normal Kalman filter, the adaptive Kalman filter provides online estimation of the noise covariance matrix based on online stochastic modelling [32,33,31]. This paper proposes a new adaptive covariance matrix of \hat{R}_k that changes in real time accompanied by an average filter algorithm. Firstly, the innovation term is defined as follows.

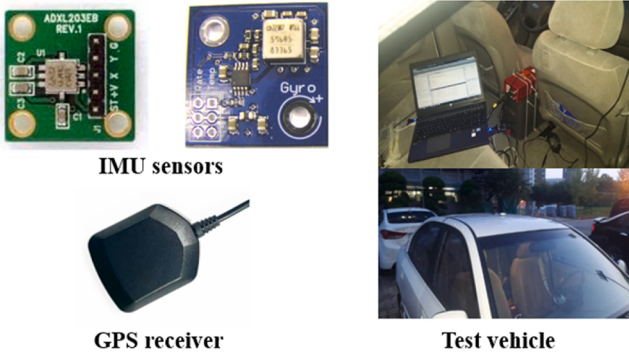


Fig. 3. Experimental set-up.

$$d_k = y_k - h(\hat{x}_k^-) \approx H_k(x_k - \hat{x}_k^-) + v_k \quad (26)$$

Taking the variances on both sides of (26), The theoretical covariance of the innovation term is given by:

$$E\{d_k d_k^T\} \approx H_k P_k^- H_k^T + R_k. \quad (27)$$

Next, the online estimation of R_k is derived through the following procedure, and the definition of the residual sequence is

$$\begin{aligned} e_k &= y_k - h(\hat{x}_k^+) = d_k + h(\hat{x}_k^-) - h(\hat{x}_k^+) \\ &\approx d_k + H_k \hat{x}_k^- - H_k (\hat{x}_k^- + K_k d_k) = (I - H_k K_k) d_k. \end{aligned} \quad (28)$$

Taking the variances on both sides of (28), the theoretical covariance of the residual can be expressed as follows.

$$\begin{aligned} E\{e_k e_k^T\} &\approx (I - H_k K_k)(H_k P_k^- H_k^T + R_k)(I - H_k K_k)^T \\ &= R_k + H_k K_k H_k P_k^- H_k^T - H_k P_k^- H_k^T \\ &= R_k + H_k (K_k H_k P_k^- + P_k^-) H_k^T = R_k - H_k P_k^+ H_k^T \end{aligned} \quad (29)$$

In practice, $E\{e_k e_k^T\}$ can be obtained through average filter algorithm over a moving window of an appropriate size m . At this time, instead of a batch expression that requires storing all data within the moving window, an efficient recursive expression method that uses only the average value of the previous step and the current value is utilized. The average of the product of residual sequence ($\sigma_k = e_k e_k^T$) from time step $k-m+1$ to k is given as

$$\bar{\sigma}_k = \frac{\sigma_{k-m+1} + \sigma_{k-m+2} + \dots + \sigma_k}{m} \quad (30)$$

$$\frac{m}{m-1} \bar{\sigma}_k = \frac{\sigma_{k-m+1} + \sigma_{k-m+2} + \dots + \sigma_{k-1} + \sigma_k}{m-1} = \bar{\sigma}_{k-1} + \frac{1}{m-1} \sigma_k. \quad (31)$$

This $\bar{\sigma}_k$ at the time step k can be expressed as follows.

$$\bar{\sigma}_k = \frac{m-1}{m} \bar{\sigma}_{k-1} + \frac{1}{m} \sigma_k \quad (32)$$

By substituting $\bar{\sigma}_k$ in (32) for $E\{e_k e_k^T\}$ in (29), the adaptive covariance

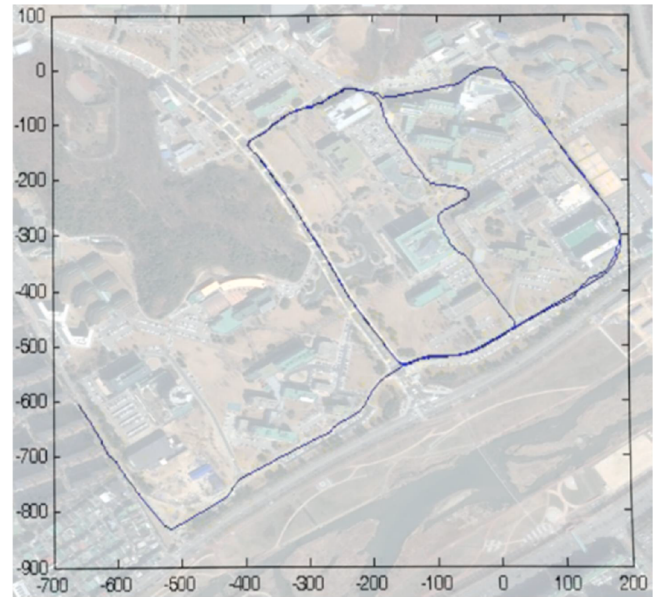


Fig. 4. Test drive course.

matrix of the measurement noise based on the average filter algorithm can be adopted:

$$\hat{R}_k = \frac{m-1}{m} \bar{\sigma}_{k-1} + \frac{1}{m} \sigma_k + H_k P_k^+ H_k^T. \quad (33)$$

At this time, the covariance matrix Q_k is regarded as a nominal value during this online estimation of R_k . Such online estimation of the \hat{R}_k is intended to be activated only in a GPS outage condition in which the accuracy of GPS measurements rapidly decreases. For this purpose, the GPS outage condition has to be accurately determined. As mentioned in Section II, GPS signal outages can be detected in real time using both NS and HDOP. In this paper, the GPS outage condition is low NS below a constant threshold NS_{low} (=5) or high HDOP above a constant threshold $HDOP_{up}$ (=5) [34–36].

5. Experimental results

Fig. 3 shows the experimental environments used to derive the experimental results in this paper. Both the standalone GPS receiver and the GPS antenna of RT3100 are placed on the center of the test vehicle roof. The RT3100 is mounted at CG of the test vehicle. The measurements from the RT3100 are considered to be the actual values. (the sampling time of the RT3100 is 0.01 s). Also, the IMU sensors are located at the center of the vehicle as much as possible so that they can measure accelerations and angular rates relative to the vehicle CG. In Table 2, main specifications of each sensor used in this paper are summarized: root mean square (RMS) and circular error probability (CEP).

The test drive course for experiments is selected as an urban area consisting of several buildings and normal roads including straight

Table 2
Main specifications of each sensor.

Sensor		Sampling rate	Measurement accuracy (output noise)	Measurement range
IMU sensors	accelerometer (ADXL203) Gyroscope (ADW22307)	100 Hz	$1.4 \times 10^{-3} \text{ m/s}^2$ (RMS) 0.5 deg/s (RMS)	$-17 \sim 17 \text{ m/s}^2$ $-250 \sim 250 \text{ deg/s}$
Standalone GPS (MiniGmouse)	1 Hz	position : 3.0 m (50 % CEP) velocity : 0.1 m/s (RMS) course angle : 0.5 deg (RMS)	N/A	
Verification equipment (RT3100)	100 Hz	position : 0.4 m (50 % CEP) velocity : $2.78 \times 10^{-2} \text{ m/s}$ (RMS) yaw angle : 0.05 deg (RMS)		

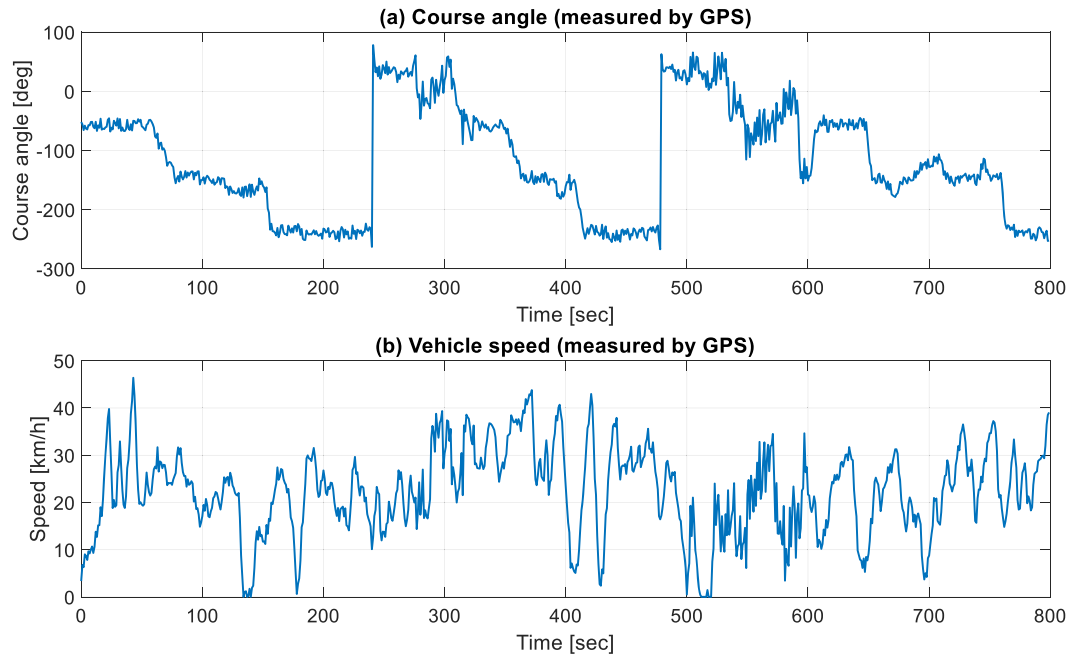


Fig. 5. GPS measurements: (a) Course angle and (b) Vehicle speed.

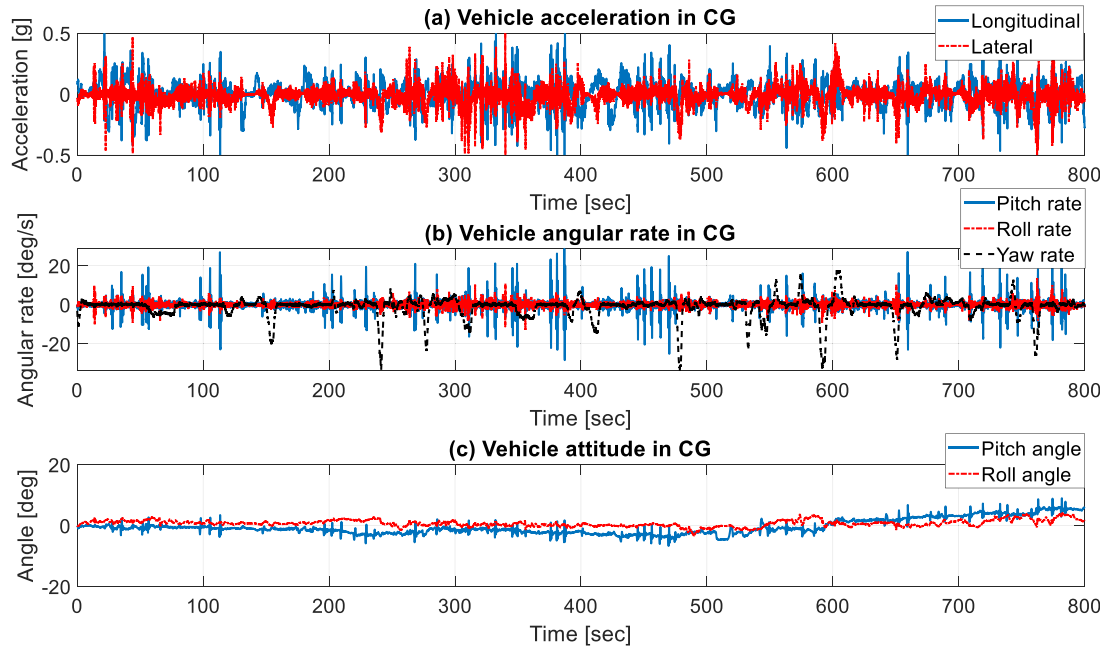


Fig. 6. (a) Vehicle accelerations, (b) Vehicle angular rates and (c) Vehicle attitudes.

roads, curves and intersections. Fig. 4 shows a map of the actual driving course from Google Earth.

The speed of the vehicle represents an ever-changing trajectory that is widely distributed from a standstill to a maximum of 50 km/h. Also, the entire test for 800 s is divided into 4 sections for precise error analysis. Both course angle and vehicle speed measured from the standalone GPS during the entire test are plotted in Fig. 5. Since the range of course angle is set between -270 and 90 deg in this paper, as shown in Fig. 5(a), the rapid change in course angle at about 240 s and 480 s indicates a change from -270 deg to 90 deg.

The vehicle accelerations and angular rates in vehicle CG measured from the IMU sensors at the same time are shown in Figs. 6(a) and (b), respectively. As can be seen in the Fig. 6(a), the longitudinal and lateral

accelerations of the vehicle are all distributed between -0.5 g and 0.5 g, which corresponds to the range of vehicle acceleration that is generally used intensively in city driving. During the experimental test, the test vehicle performs both gentle and rapid acceleration and deceleration situations, and both mild and sharp cornering situations can be found during the experimental test.

In order to obtain the attitude of the vehicle, i.e. the roll and pitch angles, the integration of roll rate and pitch rate in Fig. 6(b) is performed. At this time, a high pass filter is applied to prevent the integral drift caused by the sensor offset, so that the sensor offset component corresponding to the very low frequency range is filtered out. Fig. 6(c) shows the roll and pitch angles at once during this experimental test.

The GPS outage section where GPS signal reception is adversely

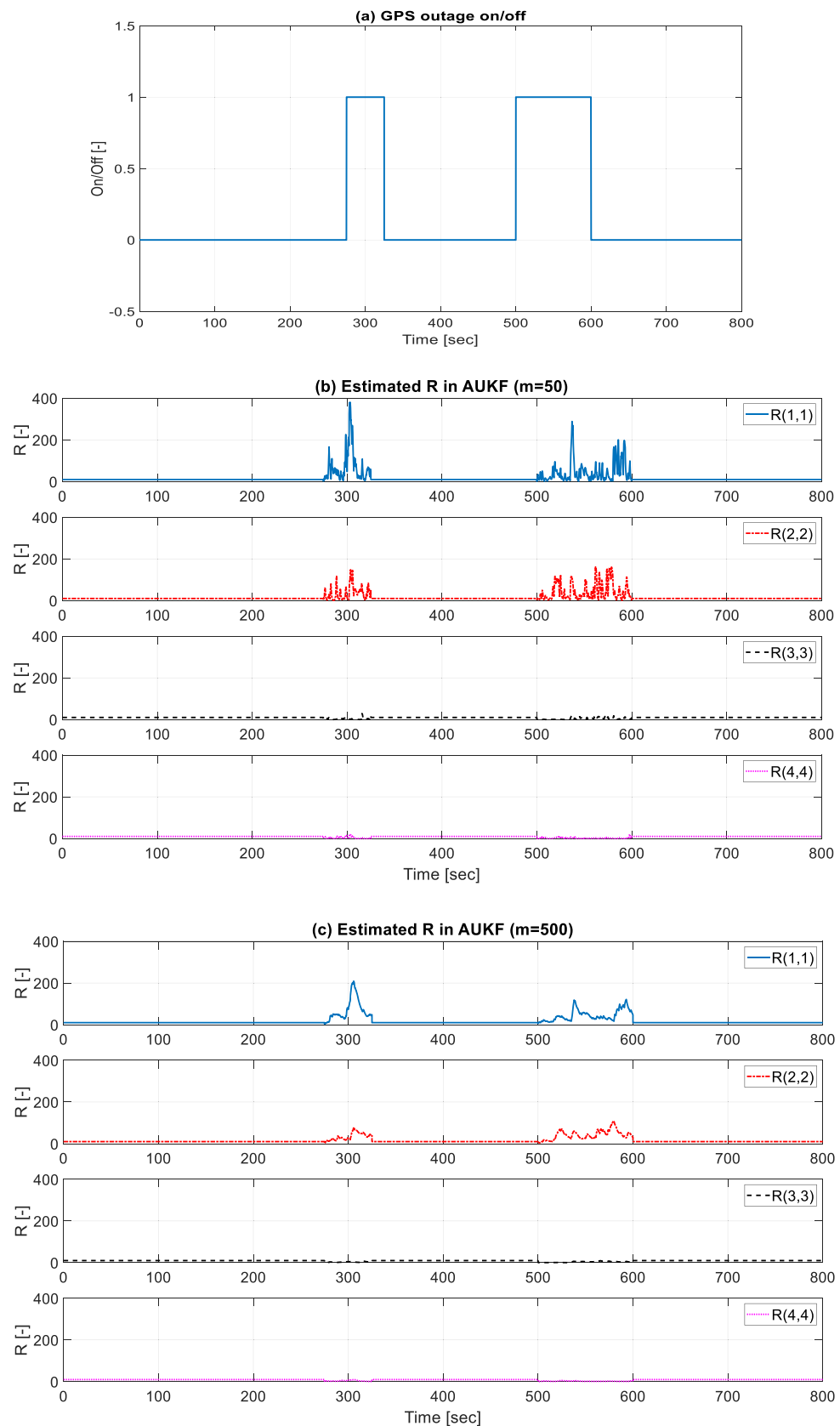


Fig. 7. Adaptive covariance matrix: (a) GPS outage detection, Estimated R in AUKF with the moving window size of (b) $m = 50$, (c) $m = 500$, and (d) $m = 1000$.

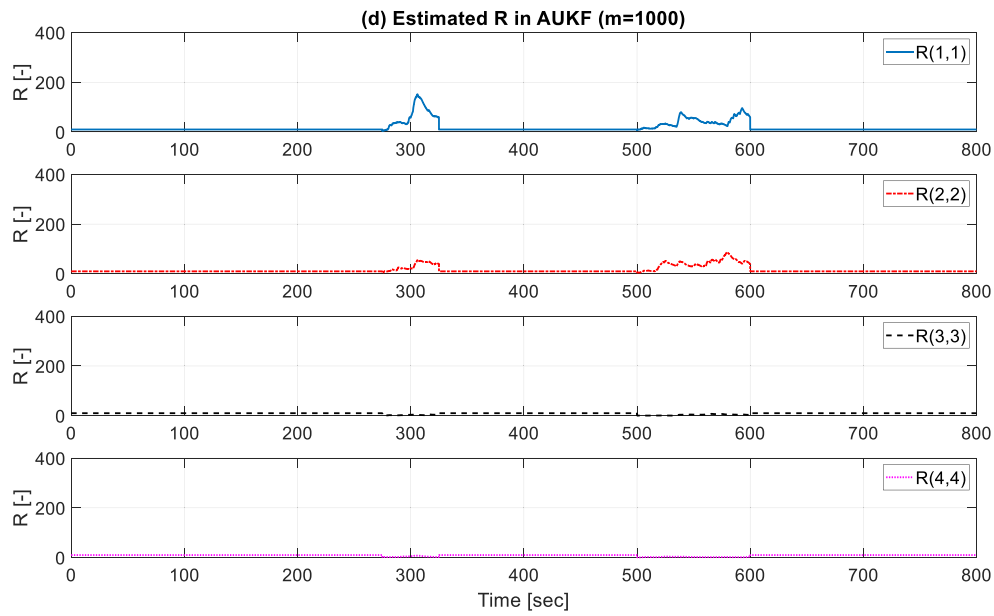


Fig. 7. (continued).

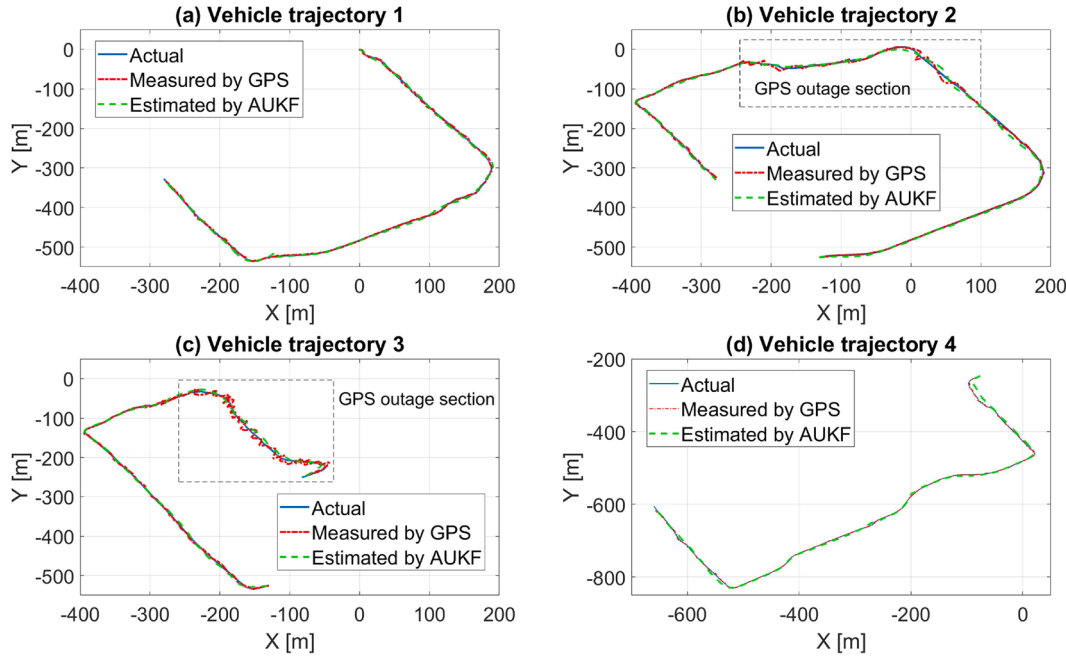


Fig. 8. Vehicle positioning results in experiments.

affected by being surrounded by tall buildings is detected as shown in Fig. 7(a) (0: GPS outage off / 1: GPS outage on). Accordingly, the estimation of R is activated only under the GPS outage condition, and Figs. 7(b), (c), and (d) show the estimation results of the adaptive covariance matrix according to different moving window sizes m , respectively. Especially, each diagonal element of the adaptive covariance matrix \hat{R}_k is illustrated at once. As can be seen in Fig. 7, the smaller m is, the rapidly changing elements of \hat{R}_k are derived. This means that the residual e_k ($= y_k - h(\hat{x}_k^+)$) is reflected more quickly in real time. However, if the moving window size m becomes too small, it is expected that \hat{R}_k with a very noisy value will be derived because it reacts too sensitively to the residual. In this paper, through pre-simulation work, we set an appropriate moving window size to $m = 50$.

Fig. 8 presents the actual vehicle position obtained from RT3100, the measured value from the standalone GPS, and the estimated value from the proposed AUKF algorithm together. It shows the entire test course in Fig. 4 divided into 4 sections and it includes several driving environments, such as curved roads, straight roads, and GPS outages. At this time, no separate reset of the distance error or estimation result occurs in each sub-section.

As shown in the trajectories on the curved roads, the estimated vehicle positions from the AUKF are quite close to the actual values, while the GPS measurement values have large errors due to its too low sampling rate to reflect the rapid vehicle behaviour changes. In addition, in the trajectories with the straight courses, the AUKF reduces these errors effectively while the GPS measurement values drift due to the multipath GPS signal problem.

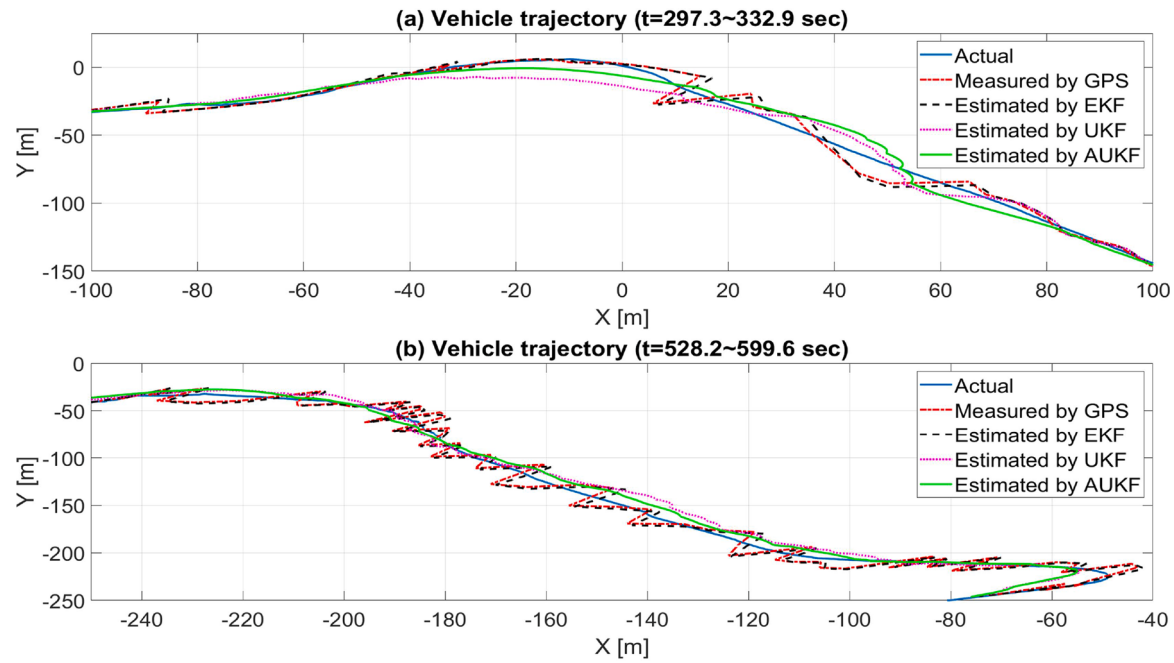


Fig. 9. Comparison between different vehicle positioning methods on GPS outage conditions.

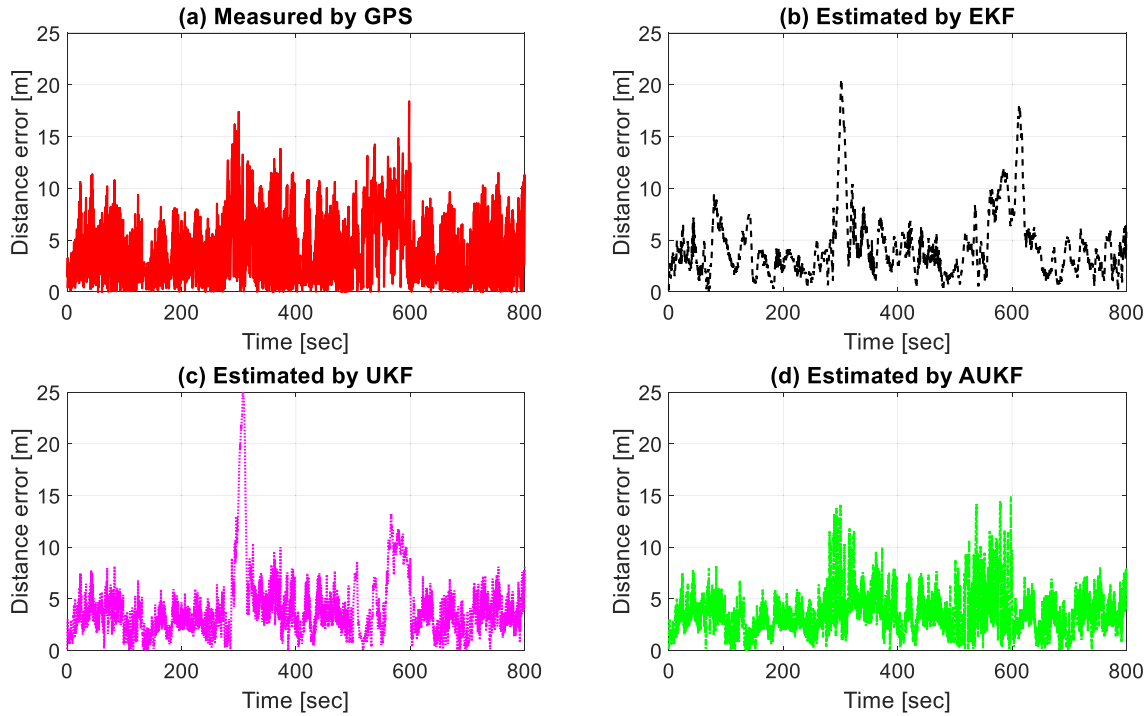


Fig. 10. Results of Euclidean distance error: (a) Measured by GPS, (b) Estimated by EKF, (c) Estimated by UKF and (d) Estimated by AUKF.

Table 3
Euclidean distance errors of each method.

Method	Case 1 0~200 s		Case 2 200 ~ 400 s		Case 3 400 ~ 600 s		Case 4 600 ~ 800 s	
	RMS [m]	Max [m]	RMS [m]	Max [m]	RMS [m]	Max [m]	RMS [m]	Max [m]
Measured by GPS	3.749	11.335	5.218	17.372	5.915	18.377	3.943	11.460
Estimated by EKF	4.028	9.458	6.008	20.529	5.342	12.073	5.461	17.898
Estimated by UKF	3.150	8.146	6.911	25.340	5.438	13.265	3.343	8.867
Estimated by AUKF (proposed)	3.150	8.146	4.539	14.171	4.988	14.887	3.337	8.867

For a detailed comparison with the existing estimation algorithms, EKF and UKF, Fig. 9 shows the vehicle position estimation results of each algorithm on GPS outage conditions. The proposed AUKF rapidly increases the magnitude of each element of the adaptive covariance matrix \hat{R}_k in these GPS outage sections, and thus estimates the vehicle position while rapidly lowering the weight of GPS measurement values and increasing the weight of the vehicle kinematic model. It implies that the AUKF automatically lowers the use of the standalone GPS and increases the use of IMU sensors on GPS outage conditions. As a result, the AUKF derives the vehicle position estimation value closest to the actual value on average compared to other estimation methods in Fig. 9.

Fig. 10 shows the Euclidean distance errors based on the actual vehicle position during the entire test period: four different types of vehicle positioning method are 1) the measurement from standalone GPS, 2) EKF, 3) UKF, and 4) AUKF (proposed). Also, regarding the results shown in Fig. 10, Table 3 shows the RMS errors and maximum errors of each method. Here, the entire test section is divided into 4 cases for detailed error analysis. In the GPS outage sections (around 300 and 600 s), the maximum errors of values directly measured from the standalone GPS are recorded as 17.372 m and 18.377 m, respectively.

By omitting the linearization process of EKF, UKF can prevent the risk of diverging estimated values due to inaccuracies in linear modeling, and thus tends to exhibit higher estimation accuracy in nonlinear systems [37]. As shown in Table 3, in normal GPS reception sections such as cases 1 and 4, UKF shows lower RMS and max distance errors than EKF. However, in GPS outage sections such as cases 2 and 3 where the accuracy of GPS measurements is not guaranteed, the estimation accuracy of UKF is no longer guaranteed.

Since both EKF and UKF use the constant measurement noise covariance matrix R_k in the corresponding section, vehicle position estimation is performed with the proportion of inaccurate GPS measurement values still high. Accordingly, they generate a very large maximum error in the GPS outage sections (in particular, refer to the maximum errors of EKF and UKF in case 2). On the other hand, the AUKF proposed in this paper leads to a significantly reduced maximum error in most sections. Additionally, the proposed AUKF tends to have a lower RMS error than EKF and UKF throughout real-vehicle experiments.

6. Conclusion

This paper introduces a new method for vehicle position estimation constructed with AUKF based on sensor fusion between standalone GPS and IMU sensors. For the nonlinear vehicle kinematic model, AUKF,

which is a combination of a general UKF and an adaptive covariance matrix that changes depending on the situation, is applied. Real-vehicle experiments are conducted on a test course that includes various driving conditions such as curved roads, straight roads, and GPS outage sections. Through this, it can be confirmed that the proposed AUKF has better estimation performance than other estimation algorithms such as general UKF and general EKF.

The main contributions of the proposed vehicle positioning algorithm are summarized as follows. 1) In a GPS outage section where the GPS measurement accuracy is severely reduced, the AUKF can output an estimated vehicle position with a very low weight to the GPS measurement value while automatically increasing the value of the covariance matrix of the GPS measurement error. 2) By applying an average filter to the adaptive covariance matrix, how smoothly and quickly it changes can be adjusted. 3) By considering roll and pitch motions together, the AUKF is accompanied by more sophisticated vehicle kinematic model.

Finally, the proposed AUKF can output robust and accurate vehicle position estimation results even for model nonlinearity and GPS outage sections. Based on these results, it is expected that it will be able to contribute to improving the performance of vehicle position recognition systems in autonomous vehicles in the future.

CRediT authorship contribution statement

Giseo Park: Conceptualization, Methodology, Software, Data curation, Writing – original draft, Visualization, Supervision, Validation, Writing – review & editing.

Declaration of competing interest

The authors declare that they have no known competing financial interests or personal relationships that could have appeared to influence the work reported in this paper.

Data availability

No data was used for the research described in the article.

Acknowledgement

This research was supported by the 2024 Research Fund of University of Ulsan.

Appendix A

Equation (A.1 and A.2)

$$\frac{\partial L_f^{(0)}}{\partial x} = \frac{\partial h}{\partial x} = \begin{bmatrix} 1 & 0 & 0 & 0 & 0 \\ 0 & 1 & 0 & 0 & 0 \\ 0 & 0 & \sin(\psi) & \cos(\psi) & v_x \cos(\psi) - v_y \sin(\psi) \\ 0 & 0 & \cos(\psi) & -\sin(\psi) & -v_x \sin(\psi) - v_y \cos(\psi) \end{bmatrix} \quad (\text{A.1})$$

$$O = \begin{bmatrix} \frac{\partial L_f^{(0)}}{\partial x} \\ \frac{\partial L_f^{(1)}}{\partial x} \\ \vdots \\ \frac{\partial L_f^{(n-1)}}{\partial x} \end{bmatrix} = \begin{bmatrix} 1 & 0 & 0 & 0 & 0 \\ 0 & 1 & 0 & 0 & 0 \\ 0 & 0 & \sin(\psi) & \cos(\psi) & v_x \cos(\psi) - v_y \sin(\psi) \\ 0 & 0 & \cos(\psi) & -\sin(\psi) & -v_x \sin(\psi) - v_y \cos(\psi) \\ \vdots & \vdots & \vdots & \vdots & \vdots \end{bmatrix} \quad (\text{A.2})$$

References

- [1] Bevly DM. Global positioning system (GPS): a low-cost velocity sensor for correcting inertial sensor errors on ground vehicles. ASME J Dyn Syst, Meas, Control 2004;126(2):255–64.
- [2] Li X, Chen W, Chan C. A reliable multisensory fusion strategy for land vehicle positioning using low cost sensors. IMechE Part D: J Automob Engin 2014;228(12):1375–97.
- [3] Jo K, Chu K, Sunwoo M. Interacting multiple model filter-based sensor fusion of GPS with in-vehicle sensors for real-time vehicle positioning. IEEE Trans Intell Transp Syst 2012;13(1):329–43.
- [4] Park G, Hwang Y, Choi S. Vehicle positioning based on velocity and heading angle observer using low-cost sensor fusion. ASME J Dyn Syst, Meas, Control 2017;139(12):1–13.
- [5] Yoon J, Peng H. A cost-effective sideslip estimation method using velocity measurements from two GPS receivers. IEEE Trans Vehi Technol 2014;63(6):2589–99.
- [6] Katriniok A, Abel D. Adaptive EKF-based vehicle state estimation with online assessment of local observability. IEEE Trans Control Syst Technol 2016;24(4):1368–81.
- [7] Leung K, Whidborne J, Purdy D, Barber P. Road vehicle sate estimation using low-cost GPS/INS. Mech Sys Sig Process 2011;25(6):1988–2004.
- [8] Boada B, Boada M, Diaz V. Vehicle sideslip angle measurement based on sensor data fusion using an integrated ANFIS and an unscented Kalman filter algorithm. Mech Sys Sig Proc 2016;72–73:832–45.
- [9] Wu Z, Yao M, Ma H, Jia W. Improving accuracy of the vehicle attitude estimation for low-cost INS/GPS integration aided by the GPS-measured course angle. IEEE Trans Intell Transport Syst 2013;14(2):553–64.
- [10] Yang Y, Gu Z, Hu L. Research on the information fusion method of the global positioning system-dead reckoning vehicle integrated navigation system. IMechE Part D: J Automob Engin 2007;221(5):543–53.
- [11] Bonnabel S, Salaun E. Design and prototyping of a low-cost vehicle localization system with Guaranteed convergence properties. Control Eng Pract 2011;19(6):591–601.
- [12] Chiang KW, Duong T, Liao JK. The performance analysis of a real-time integrated INS/GPS vehicle navigation system with abnormal GPS measurement elimination. Sensors 2013;13(8):10599–622.
- [13] Wang S, Deng Z, Yin G. An accurate GPS-IMU/DR data fusion method for driverless car based on a set of predictive models and grid constraints. Sensors 2016;16(3):280.
- [14] Xiao Z, Havyarimana V, Li T, Wang D. A nonlinear framework of delayed particle smoothing method for vehicle localization under non-Gaussian environment. Sensors 2016;16(5):692.
- [15] Belhajem I, Maissa YB, Tamtaoui A. Improving low cost sensor based vehicle positioning with machine learning. Control Eng Pract 2018;74:168–76.
- [16] Gruyer D, Pollard E. Credibilistic IMM likelihood updating applied to outdoor vehicle robust ego-localization. In: 14th International Conference on Information Fusion; 2011.
- [17] Jo K, Lee M, Sunwoo M. Road slope aided vehicle position estimation system based on sensor fusion of GPS and automotive onboard sensors. IEEE Trans Intell Trans Syst 2016;17(1):250–63.
- [18] Xu Q, Li X, Chan C. A cost-effective vehicle localization solution using an interacting multiple model–unscented Kalman filters (IMM-UKF) algorithm and grey neural network. Sensors 2017;17(6):1431.
- [19] Godoy J, Gruyer D, Lambert A, Villagra J. Development of an particle swarm algorithm for vehicle localization. In: 2012 IEEE Intelligent Vehicles Symposium; 2012.
- [20] Bacha ARA, Gruyer D, Lambert A. A performance test for a new reactive-cooperative filter in an ego-vehicle localization application. In: 2014 IEEE Intelligent Vehicles Symposium; 2014.
- [21] Choi M, Seo M, Kim H, Seo T. UKF-based sensor fusion method for position estimation of a 2-DOF Rope driven robot. IEEE Access 2021;9:12301–8.
- [22] Bucci A, Franchi M, Ridolfi A, Secciani N, Allotta B. Evaluation of UKF-based fusion strategies for autonomous underwater vehicles multisensor navigation. IEEE J Ocean Engin 2023;48(1):1–26.
- [23] Peng J, Zhang P, Zheng L, Tan J. UAV positioning based on multi-sensor fusion. IEEE Access 2020;8:34455–67.
- [24] Franchi M, Ridolfi A, Allotta B. Underwater navigation with 2D forward looking SONAR: an adaptive unscented Kalman filter-based strategy for AUVs. J Field Robot 2021;38(3):355–85.
- [25] Song Q, Qi J, Han J. An adaptive UKF algorithm and its application in mobile robot control. In: 2006 IEEE International Conference on Robotics and Biomimetics; 2006.
- [26] Liu J, Lu M. An adaptive UKF filtering algorithm for GPS position estimation. In: 2009 5th International Conference on Wireless Communications, Networking and Mobile Computing; 2009.
- [27] Oh J, Choi S. Vehicle velocity observer design Using 6-D IMU and multiple-observer Approach. IEEE Trans Intell Trans Syst 2012;13(4):1865–79.
- [28] Fiengo G, Domenico DD, Glielmo L. A hybrid procedure strategy for vehicle localization system: design and prototyping. Control Eng Pract 2009;17(1):14–25.
- [29] Meguro J, Kojima Y, Suzuki N, Teramoto E. Positioning technique based on vehicle trajectory using GPS raw data and low-cost IMU. Int J Auto Eng 2012;3:75–80.
- [30] Yoon JH, Li SE, Ahn C. Estimation of vehicle sideslip angle and tire-road friction coefficient based on magnetometer with GPS. Int J Auto Technol 2016;17(3):427–35.
- [31] Ding W, Wang J, Rizos C. Improving adaptive Kalman estimation in GPS/INS integration. J Navigat 2007;60(3):517–29.
- [32] Mehra R. On the identification of variances and adaptive Kalman filtering. IEEE Trans Auto Con 1970;15(2):175–84.
- [33] Almagbile A, Wang J, Ding W. Evaluating the performances of adaptive Kalman filter methods in GPS/INS integration. J Glob Posit Sys 2010;9(1):33–40.
- [34] Mohamed AH, Schwarz KP. Adaptive Kalman filtering for INS/GPS. J Geod 1999;73(4):193–203.
- [35] Beiker SA, Gaubatz KH, Gerdes JC, Rock KL. GPS augmented vehicle dynamics control. SAE transactions. 2006. p. 1174–82.
- [36] Langley RB. Dillution of precision. GPS world. Canada: New Brunswick; 1999.
- [37] Chang L, Hu B, Li A, Qin F. Transformed unscented Kalman filter. IEEE Trans Autom Cont 2012;58(1):252–7.



Giseo Park received the B.S. degree in mechanical engineering from Hanyang University, Seoul, Korea, in 2014 and the M.S. and Ph.D. degrees in mechanical engineering from Korea Advanced Institute of Science and Technology (KAIST), in 2016 and 2020. He was a senior engineer with Hyundai Motor Company, Hwasung, South Korea. He has been an assistant professor in the school of mechanical engineering from University of Ulsan, Ulsan, Korea. His research interests include vehicle dynamics, control theory, active safety systems and autonomous driving system.